

Submitted to: EPJC

First proton–proton collisions at the LHC as observed with the ALICE detector: measurement of the charged-particle pseudorapidity density at $\sqrt{s} = 900$ GeV

ALICE Collaboration

Abstract

On 23rd November 2009, during the early commissioning of the CERN Large Hadron Collider (LHC), two counter-rotating proton bunches were circulated for the first time concurrently in the machine, at the LHC injection energy of 450 GeV per beam. Although the proton intensity was very low, with only one pilot bunch per beam, and no systematic attempt was made to optimize the collision optics, all LHC experiments reported a number of collision candidates. In the ALICE experiment, the collision region was centred very well in both the longitudinal and transverse directions and 284 events were recorded in coincidence with the two passing proton bunches. The events were immediately reconstructed and analyzed both online and offline. We have used these events to measure the pseudorapidity density of charged primary particles in the central region. In the range $|\eta| < 0.5$, we obtain $dN_{\text{ch}}/d\eta = 3.10 \pm 0.13(\text{stat.}) \pm 0.22(\text{syst.})$ for all inelastic interactions, and $dN_{\text{ch}}/d\eta = 3.51 \pm 0.15(\text{stat.}) \pm 0.25(\text{syst.})$ for non-single diffractive interactions. These results are consistent with previous measurements in proton–antiproton interactions at the same centre-of-mass energy at the CERN Sp \bar{p} S collider. They also illustrate the excellent functioning and rapid progress of the LHC accelerator, and of both the hardware and software of the ALICE experiment, in this early start-up phase.

First proton–proton collisions at the LHC as observed with the ALICE detector: measurement of the charged-particle pseudorapidity density at $\sqrt{s} = 900$ GeV

ALICE collaboration

K. Aamodt⁷⁸, N. Abel⁴³, U. Abeysekera³⁰, A. Abrahamtes Quintana⁴², A. Acero⁶³, D. Adamová⁸⁶, M.M. Aggarwal²⁵, G. Aglieri Rinella⁴⁰, A.G. Agocs¹⁸, S. Aguilar Salazar⁶⁶, Z. Ahammed⁵⁵, A. Ahmad², N. Ahmad², S.U. Ahn⁵⁰ⁱ, R. Akimoto¹⁰⁰, A. Akimov⁶⁸, D. Aleksandrov⁷⁰, B. Alessandro¹⁰², R. Alfaro Molina⁶⁶, A. Alici¹³, E. Almaráz Aviña⁶⁶, J. Alme⁸, T. Alt⁴³ⁱⁱ, V. Altini⁶, S. Altinpinar³², C. Andrei¹⁷, A. Andronic³², G. Anelli⁴⁰, V. Angelov⁴³ⁱⁱ, C. Anson²⁷, T. Antičić¹¹³, F. Antinori⁴⁰ⁱⁱⁱ, S. Antinori¹³, K. Antipin³⁷, D. Antończyk³⁷, P. Antonioli¹⁴, A. Anzo⁶⁶, L. Aphecetche⁷³, H. Appelshäuser³⁷, S. Arcelli¹³, R. Arceo⁶⁶, A. Arend³⁷, N. Armesto⁹², R. Arnaldi¹⁰², T. Aronsson⁷⁴, I.C. Arsene^{78iv}, A. Asryan⁹⁸, A. Augustinus⁴⁰, R. Averbeck³², T.C. Awes⁷⁶, J. Äystö⁴⁹, M.D. Azmi², S. Bablok⁸, M. Bach³⁶, A. Badalà²⁴, Y.W. Baek⁵⁰ⁱ, S. Bagnasco¹⁰², R. Bailhache^{32v}, R. Bala¹⁰¹, A. Baldisseri⁸⁹, A. Baldit²⁶, J. Bán⁵⁸, R. Barbera²³, G.G. Barnaföldi¹⁸, L. Barnby¹², V. Barret²⁶, J. Bartke²⁹, F. Barile⁵, M. Basile¹³, V. Basmanov⁹⁴, N. Bastid²⁶, B. Bathen⁷², G. Batigne⁷³, B. Batyunya³⁵, C. Baumann^{72v}, I.G. Bearden²⁸, B. Becker^{20vi}, I. Belikov⁹⁹, R. Bellwied³⁴, E. Belmont-Moreno⁶⁶, A. Belogianni⁴, L. Benhabib⁷³, S. Beole¹⁰¹, I. Berceau¹⁷, A. Bercuci^{32vii}, E. Berdermann³², Y. Berdnikov³⁹, L. Betev⁴⁰, A. Bhasin⁴⁸, A.K. Bhati²⁵, L. Bianchi¹⁰¹, N. Bianchi³⁸, C. Bianchin⁷⁹, J. Bielčík⁸¹, J. Bielčíková⁸⁶, A. Bilandžić³, L. Bimbot⁷⁷, E. Biolcati¹⁰¹, A. Blanc²⁶, F. Blanco^{23viii}, F. Blanco⁶³, D. Blau⁷⁰, C. Blume³⁷, M. Boccioni⁴⁰, N. Bock²⁷, A. Bogdanov⁶⁹, H. Bøggild²⁸, M. Bogolyubsky⁸³, J. Bohm⁹⁶, L. Boldizsár¹⁸, M. Bombara^{12ix}, C. Bombonati^{79x}, M. Bondila⁴⁹, H. Borel⁸⁹, V. Borshchov⁵¹, C. Bortolin⁷⁹, S. Bose⁵⁴, L. Bosisio¹⁰³, F. Bossu¹⁰¹, M. Botje³, S. Böttger⁴³, G. Bourdaud⁷³, B. Boyer⁷⁷, M. Braun⁹⁸, P. Braun-Munzinger^{32,33ii}, L. Bravina⁷⁸, M. Bregant^{103xi}, T. Breitner⁴³, G. Bruckner⁴⁰, R. Brun⁴⁰, E. Bruna⁷⁴, G.E. Bruno⁵, D. Budnikov⁹⁴, H. Buesching³⁷, K. Bugaev⁵², P. Buncic⁴⁰, O. Busch⁴⁴, Z. Buthelezi²², D. Caffarri⁷⁹, X. Cai¹¹¹, H. Caines⁷⁴, E. Camacho⁶⁴, P. Camerini¹⁰³, M. Campbell⁴⁰, V. Canoa Roman⁴⁰, G.P. Capitani³⁸, G. Cara Romeo¹⁴, F. Carena⁴⁰, W. Carena⁴⁰, F. Carminati⁴⁰, A. Casanova Díaz³⁸, M. Caselle⁴⁰, J. Castillo Castellanos⁸⁹, J.F. Castillo Hernandez³², V. Catanescu¹⁷, E. Cattaruzza¹⁰³, C. Cavicchioli⁴⁰, P. Cerello¹⁰², V. Chambert⁷⁷, B. Chang⁹⁶, S. Chapeland⁴⁰, A. Charpy⁷⁷, J.L. Charvet⁸⁹, S. Chattopadhyay⁵⁴, S. Chattopadhyay⁵⁵, M. Cherney³⁰, C. Cheshkov⁴⁰, B. Cheynis⁶², E. Chiavassa¹⁰¹, V. Chibante Barroso⁴⁰, D.D. Chinellato²¹, P. Chochula⁴⁰, K. Choi⁸⁵, M. Chojnacki¹⁰⁶, P. Christakoglou¹⁰⁶, C.H. Christensen²⁸, P. Christiansen⁶¹, T. Chujo¹⁰⁵, F. Chuman⁴⁵, C. Cicalo²⁰, L. Cifarelli¹³, F. Cindolo¹⁴, J. Cleymans²², O. Cobanoglu¹⁰¹, J.-P. Coffin⁹⁹, S. Coli¹⁰², A. Colla⁴⁰, G. Conesa Balbastre³⁸, Z. Conesa del Valle^{73xii}, E.S. Conner¹¹⁰, P. Constantin⁴⁴, G. Contin^{103x}, J.G. Contreras⁶⁴, Y. Corrales Morales¹⁰¹, T.M. Cormier³⁴, P. Cortese¹, I. Cortés Maldonado⁸⁴, M.R. Cosentino²¹, F. Costa⁴⁰, M.E. Cotallo⁶³, E. Crescio⁶⁴, P. Crochet²⁶, E. Cuautle⁶⁵, L. Cunqueiro³⁸, J. Cussonneau⁷³, A. Dainese⁵⁹ⁱⁱⁱ, H.H. Dalsgaard²⁸, A. Danu¹⁶, I. Das⁵⁴, S. Das⁵⁴, A. Dash¹¹, S. Dash¹¹, G.O.V. de Barros⁹³, A. De Caro⁹⁰, G. de Cataldo^{40xiii}, J. de Cuveland⁴³ⁱⁱ, A. De Falco¹⁹, M. de Gaspari⁴⁴, J. de Groot⁴⁰, D. De Gruttola⁹⁰, A.P. de Haas¹⁰⁶, N. De Marco¹⁰², R. de Rooij¹⁰⁶, S. De Pasquale⁹⁰, G. de Vaux²², H. Delagrèze⁷³, G. Dellacasa¹, A. Deloff¹⁰⁷, V. Demanov⁹⁴, E. Dénes¹⁸, A. Deppman⁹³, G. D'Erasmus⁵, D. Derkach⁹⁸, A. Devaux²⁶, D. Di Bari⁵, C. Di Giglio^{5x}, S. Di Liberto⁸⁸, A. Di Mauro⁴⁰, P. Di Nezza³⁸, M. Dialinas⁷³, L. Díaz⁶⁵, R. Díaz⁴⁹, T. Dietel⁷², H. Ding¹¹¹, R. Divià⁴⁰, Ø. Djuvsland⁸, G. do Amaral Valdivieso²¹, V. Dobretsov⁷⁰, A. Dobrin⁶¹, T. Dobrowolski¹⁰⁷, B. Dönigus³², I. Domínguez⁶⁵, D.M.M. Don⁴⁶, O. Dordic⁷⁸, A.K. Dubey⁵⁵, J. Dubuisson⁴⁰, L. Ducroux⁶², P. Dupieux²⁶, A.K. Dutta Majumdar⁵⁴, M.R. Dutta Majumdar⁵⁵, D. Elia⁶, D. Emschermann^{44xiv}, A. Enokizono⁷⁶, B. Espagnon⁷⁷, M. Estienne⁷³, D. Evans¹², S. Evrard⁴⁰, G. Eyyubova⁷⁸, C.W. Fabjan^{40xv}, D. Fabris⁷⁹, J. Faivre⁴¹, D. Falchieri¹³, A. Fantoni³⁸, M. Fasel³², R. Fearick²², A. Fedunov³⁵, D. Fehler⁸, V. Fekete¹⁵, D. Felea¹⁶, B. Fenton-Olsen^{28xvi}, G. Feofilov⁹⁸, A. Fernández Téllez⁸⁴, E.G. Ferreira⁹², A. Ferretti¹⁰¹, R. Ferretti^{1xvii}, M.A.S. Figueredo⁹³, S. Filchagin⁹⁴, R. Fini⁶, F.M. Fionda⁵, E.M. Fiore⁵, M. Floris^{19x}, Z. Fodor¹⁸, S. Foertsch²², P. Foka³², S. Fokin⁷⁰, F. Formenti⁴⁰, E. Fragiaco¹⁰⁴, M. Fragkiadakis⁴, U. Frankenfeld³², A. Frolov⁷⁵, U. Fuchs⁴⁰, F. Furano⁴⁰, C. Furget⁴¹, M. Fusco Girard⁹⁰, J.J. Gaardhøje²⁸, S. Gadrat⁴¹, M. Gagliardi¹⁰¹, A. Gago^{64xviii}, M. Gallio¹⁰¹, P. Ganoti⁴, M.S. Ganti⁵⁵, C. Garabatos³², C. García Trapaga¹⁰¹, J. Gebelein⁴³, R. Gemme¹, M. Germain⁷³, A. Gheata⁴⁰, M. Gheata⁴⁰, B. Ghidini⁵, P. Ghosh⁵⁵, G. Giraudo¹⁰², P. Giubellino¹⁰², E. Gladysz-Dziadus²⁹, R. Glasow^{72xix}, P. Glässel⁴⁴, A. Glenn⁶⁰, R. Gomez³¹, H. González Santos⁸⁴,

L.H. González-Trueba⁶⁶, P. González-Zamora⁶³, S. Gorbunov⁴³ⁱⁱ, Y. Gorbunov³⁰, S. Gotovac⁹⁷, H. Gottschlag⁷², V. Grabski⁶⁶, R. Grajcarek⁴⁴, A. Grelli¹⁰⁶, A. Grigoras⁴⁰, C. Grigoras⁴⁰, V. Grigoriev⁶⁹, A. Grigoryan¹¹², B. Grinyov⁵², N. Grion¹⁰⁴, P. Gros⁶¹, J.F. Grosse-Oetringhaus⁴⁰, J.-Y. Grossiord⁶², R. Grosso⁸⁰, C. Guarnaccia⁹⁰, F. Guber⁶⁷, R. Guernane⁴¹, B. Guerzoni¹³, K. Gulbrandsen²⁸, H. Gulkanyan¹¹², T. Gunji¹⁰⁰, A. Gupta⁴⁸, R. Gupta⁴⁸, H.-A. Gustafsson⁶¹, H. Gutbrod³², Ø. Haaland⁸, C. Hadjidakis⁷⁷, M. Haiduc¹⁶, H. Hamagaki¹⁰⁰, G. Hamar¹⁸, J. Hamblen⁵³, B.H. Han⁹⁵, J.W. Harris⁷⁴, M. Hartig³⁷, A. Harutyunyan¹¹², D. Hasch³⁸, D. Hasegan¹⁶, D. Hatzifotiadou¹⁴, A. Hayrapetyan¹¹², M. Heide⁷², M. Heinz⁷⁴, H. Helstrup⁹, A. Herghelegiu¹⁷, C. Hernández³², G. Herrera Corral⁶⁴, N. Herrmann⁴⁴, K.F. Hetland⁹, B. Hicks⁷⁴, A. Hiei⁴⁵, P.T. Hille^{78xx}, B. Hippolyte⁹⁹, T. Horaguchi^{45xxi}, Y. Hori¹⁰⁰, P. Hristov⁴⁰, I. Hřivnáčová⁷⁷, S. Hu⁷, S. Huber³², T.J. Humanic²⁷, D. Hutter³⁶, D.S. Hwang⁹⁵, R. Ichou⁷³, R. Ilkaev⁹⁴, I. Ilkiv¹⁰⁷, P.G. Innocenti⁴⁰, M. Ippolitov⁷⁰, M. Irfan², C. Ivan¹⁰⁶, A. Ivanov⁹⁸, M. Ivanov³², V. Ivanov³⁹, T. Iwasaki⁴⁵, A. Jacholkowski⁴⁰, P. Jacobs¹⁰, L. Jančurová³⁵, S. Jangal⁹⁹, R. Janik¹⁵, K. Jayananda³⁰, C. Jena¹¹, S. Jena⁷¹, L. Jirden⁴⁰, G.T. Jones¹², P.G. Jones¹², P. Jovanovic¹², H. Jung⁵⁰, W. Jung⁵⁰, A. Jusko¹², A.B. Kaidalov⁶⁸, S. Kalcher⁴³ⁱⁱ, P. Kaliňák⁵⁸, T. Kalliokoski⁴⁹, A. Kalweit³³, A. Kamal², R. Kamermans¹⁰⁶, K. Kanaki⁸, E. Kang⁵⁰, J.H. Kang⁹⁶, J. Kapitan⁸⁶, V. Kaplin⁶⁹, S. Kapusta⁴⁰, T. Karavicheva⁶⁷, E. Karpechev⁶⁷, A. Kazantsev⁷⁰, U. Keschull⁴³, R. Keidel¹¹⁰, M.M. Khan², S.A. Khan⁵⁵, A. Khanzadeev³⁹, Y. Kharlov⁸³, D. Kikola¹⁰⁸, B. Kileng⁹, D.J. Kim⁴⁹, D.S. Kim⁵⁰, D.W. Kim⁵⁰, H.N. Kim⁵⁰, J. Kim⁸³, J.H. Kim⁹⁵, J.S. Kim⁵⁰, M. Kim⁵⁰, M. Kim⁹⁶, S.H. Kim⁵⁰, S. Kim⁹⁵, Y. Kim⁹⁶, S. Kirsch⁴⁰, I. Kisel^{43iv}, S. Kiselev⁶⁸, A. Kisel^{27x}, J.L. Klay⁹¹, J. Klein⁴⁴, C. Klein-Bösing^{40xiv}, M. Kliemant³⁷, A. Klovning⁸, A. Kluge⁴⁰, S. Kniege³⁷, K. Koch⁴⁴, R. Kolevatov⁷⁸, A. Kolojvari⁹⁸, V. Kondratiev⁹⁸, N. Kondratyeva⁶⁹, A. Konevskih⁶⁷, E. Kornaš²⁹, R. Kour¹², M. Kowalski²⁹, S. Kox⁴¹, K. Kozlov⁷⁰, J. Kral^{81xi}, I. Králik⁵⁸, F. Kramer³⁷, I. Kraus^{33iv}, A. Kravčáková⁵⁷, T. Krawutschke⁵⁶, M. Krivda¹², D. Krumbhorn⁴⁴, M. Krus⁸¹, E. Kryshen³⁹, M. Krzewicki³, Y. Kucheriaev⁷⁰, C. Kuhn⁹⁹, P.G. Kuijter³, L. Kumar²⁵, N. Kumar²⁵, R. Kupczak¹⁰⁸, P. Kurashvili¹⁰⁷, A. Kurepin⁶⁷, A.N. Kurepin⁶⁷, A. Kuryakin⁹⁴, S. Kushpil⁸⁶, V. Kushpil⁸⁶, M. Kutouski³⁵, H. Kvaerno⁷⁸, M.J. Kweon⁴⁴, Y. Kwon⁹⁶, P. La Rocca^{23xxii}, F. Lackner⁴⁰, P. Ladrón de Guevara⁶³, V. Lafage⁷⁷, C. Lal⁴⁸, C. Lara⁴³, D.T. Larsen⁸, G. Laurenti¹⁴, C. Lazzeroni¹², Y. Le Bornec⁷⁷, N. Le Bris⁷³, H. Lee⁸⁵, K.S. Lee⁵⁰, S.C. Lee⁵⁰, F. Lefèvre⁷³, M. Lenhardt⁷³, L. Leistam⁴⁰, J. Lehnert³⁷, V. Lenti⁶, H. León⁶⁶, I. León Monzón³¹, H. León Vargas³⁷, P. Lévai¹⁸, Y. Li⁷, R. Lietava¹², S. Lindal⁷⁸, V. Lindenstruth⁴³ⁱⁱ, C. Lippmann⁴⁰, M.A. Lisa²⁷, O. Listratenko⁵¹, L. Liu⁸, V. Loginov⁶⁹, S. Lohn⁴⁰, X. Lopez²⁶, M. López Noriega⁷⁷, R. López-Ramírez⁸⁴, E. López Torres⁴², G. Løvholden⁷⁸, A. Lozea Feijo Soares⁹³, S. Lu⁷, M. Lunardon⁷⁹, G. Luparello¹⁰¹, L. Luquin⁷³, J.-R. Lutz⁹⁹, M. Luvisetto¹⁴, K. Ma¹¹¹, R. Ma⁷⁴, D.M. Madagadahettige-Don⁴⁶, A. Maevskaya⁶⁷, M. Mager^{33x}, A. Mahajan⁴⁸, D.P. Mahapatra¹¹, A. Maire⁹⁹, I. Makhlyueva⁴⁰, D. Mal'Kevich⁶⁸, M. Malaev³⁹, I. Maldonado Cervantes⁶⁵, M. Malek⁷⁷, T. Malkiewicz⁴⁹, P. Malzacher³², A. Mamonov⁹⁴, L. Manceau²⁶, L. Mangotra⁴⁸, V. Manko⁷⁰, F. Manso²⁶, V. Manzari^{40xxiii}, Y. Mao^{111xxiv}, J. Mares⁸², G.V. Margagliotti¹⁰³, A. Margotti¹⁴, A. Marin³², I. Martashvili⁵³, P. Martinengo⁴⁰, M.I. Martínez⁸⁴, A. Martínez Davalos⁶⁶, G. Martínez García⁷³, Y. Maruyama⁴⁵, A. Marzari Chiesa¹⁰¹, S. Masciocchi³², M. Masera¹⁰¹, M. Masetti¹³, A. Masoni²⁰, L. Massacrier⁶², M. Mastrocorno⁵, A. Mastroserio^{5x}, Z.L. Matthews¹², B. Mattos Tavares²¹, A. Matyja²⁹, D. Mayani⁶⁵, G. Mazza¹⁰², M.A. Mazzoni⁸⁸, F. Meddi⁸⁷, A. Menchaca-Rocha⁶⁶, P. Mendez Lorenzo⁴⁰, M. Meoni⁴⁰, J. Mercado Pérez⁴⁴, P. Mereu¹⁰², Y. Miale¹⁰⁵, A. Michalon⁹⁹, N. Miftakhov³⁹, J. Milosevic⁷⁸, F. Minafra⁵, A. Mischke¹⁰⁶, D. Miśkowiec³², C. Mitu¹⁶, K. Mizoguchi⁴⁵, J. Mlynarz³⁴, B. Mohanty⁵⁵, L. Molnar^{18x}, M.M. Mondal⁵⁵, L. Montaña Zetina^{64xxv}, M. Monteno¹⁰², E. Montes⁶³, M. Morando⁷⁹, S. Moretto⁷⁹, A. Morsch⁴⁰, T. Moukhanova⁷⁰, V. Muccifora³⁸, E. Mudnic⁹⁷, S. Muhuri⁵⁵, H. Müller⁴⁰, M.G. Munhoz⁹³, J. Munoz⁸⁴, L. Musa⁴⁰, A. Musso¹⁰², B.K. Nandi⁷¹, R. Nania¹⁴, E. Nappi⁶, F. Navach⁵, S. Navin¹², T.K. Nayak⁵⁵, S. Nazarenko⁹⁴, G. Nazarov⁹⁴, A. Nedosekin⁶⁸, F. Nendaz⁶², J. Newby⁶⁰, A. Nianine⁷⁰, M. Nicassio^{6x}, B.S. Nielsen²⁸, S. Nikolaev⁷⁰, V. Nikolic¹¹³, S. Nikulin⁷⁰, V. Nikulin³⁹, B.S. Nilsen^{27xxvi}, M.S. Nilsson⁷⁸, F. Noferini¹⁴, P. Nomokonov³⁵, G. Nooren¹⁰⁶, N. Novitzky⁴⁹, A. Nyatha⁷¹, C. Nygaard²⁸, A. Nyiri⁷⁸, J. Nystrand⁸, A. Ochirov⁹⁸, G. Odyniec¹⁰, H. Oeschler³³, M. Oinonen⁴⁹, K. Okada¹⁰⁰, Y. Okada⁴⁵, M. Oldenburg⁴⁰, J. Oleniacz¹⁰⁸, C. Oppedisano¹⁰², F. Orsini⁸⁹, A. Ortíz Velázquez⁶⁵, G. Ortona¹⁰¹, C. Oskamp¹⁰⁶, A. Oskarsson⁶¹, F. Osmic⁴⁰, L. Österman⁶¹, P. Ostrowski¹⁰⁸, I. Otterlund⁶¹, J. Otwinowski³², G. Øvrebek⁸, K. Oyama⁴⁴, K. Ozawa¹⁰⁰, Y. Pachmayer⁴⁴, M. Pachr⁸¹, F. Padilla¹⁰¹, P. Pagano⁹⁰, G. Paic⁶⁵, F. Painke⁴³, C. Pajares⁹², S. Pal^{54xxvii}, S.K. Pal⁵⁵, A. Palaha¹², A. Palmeri²⁴, R. Panse⁴³, G.S. Pappalardo²⁴, W.J. Park³², B. Pastirčák⁵⁸, C. Pastore⁶, V. Patichio⁶, A. Pavlinov³⁴, T. Pawlak¹⁰⁸, T. Peitzmann¹⁰⁶, A. Pepato⁸⁰, H. Pereira⁸⁹, D. Peressounko⁷⁰, C. Pérez^{64xxviii}, D. Perini⁴⁰, D. Perrino^{5x}, W. Peryt¹⁰⁸, J. Peschek⁴³ⁱⁱ, A. Pesci¹⁴, V. Peskov^{65x}, Y. Pestov⁷⁵, A.J. Peters⁴⁰, V. Petráček⁸¹, A. Petridis^{43ix}, M. Petris¹⁷, P. Petrov¹², M. Petrovici¹⁷, C. Petta²³, J. Peyré⁷⁷, S. Piano¹⁰⁴, A. Piccotti¹⁰², M. Pikna¹⁵, P. Pillot⁷³, L. Pinsky⁴⁶, N. Pitz³⁷, F. Piuz⁴⁰, R. Platt¹², M. Płoskoń¹⁰, J. Pluta¹⁰⁸, T. Pocheptsov^{35xxviii}, S. Pochybova¹⁸, P.L.M. Podesta Lerma³¹, F. Poggio¹⁰¹, M.G. Poghosyan¹⁰¹, T. Poghosyan¹¹², K. Polák⁸², B. Polichtchouk⁸³, P. Polozov⁶⁸, V. Polyakov³⁹, B. Pommeresch⁸, A. Pop¹⁷, F. Posa⁵, V. Pospíšil⁸¹, B. Potukuchi⁴⁸, J. Pouthas⁷⁷, S.K. Prasad⁵⁵, R. Preghenella^{13xxii}, F. Prino¹⁰², C.A. Pruneau³⁴, I. Pshenichnov⁶⁷, G. Puddu¹⁹, P. Pujahari⁷¹, A. Pulvirenti²³, A. Punin⁹⁴, V. Punin⁹⁴, M. Putiš⁵⁷, J. Putschke⁷⁴, E. Quercigh⁴⁰, A. Rachevski¹⁰⁴, A. Rademakers⁴⁰, S. Radomski⁴⁴, T.S. Rähä⁴⁹, J. Rak⁴⁹, A. Rakotozafindrabe⁸⁹, L. Ramello¹, A. Ramírez Reyes⁶⁴, M. Rammner⁷², R. Raniwala⁴⁷, S. Raniwala⁴⁷, S. Räsänen⁴⁹, I. Rashevskaya¹⁰⁴, S. Rath¹¹, K. F. Read⁵³, J. Real⁴¹,

K. Redlich¹⁰⁷, R. Renfordt³⁷, A.R. Reolon³⁸, A. Reshetin⁶⁷, F. Rettig⁴³ⁱⁱ, J.-P. Revol⁴⁰, K. Reygers^{72xxix}, H. Ricaud^{99xxx}, L. Riccati¹⁰², R.A. Ricci⁵⁹, M. Richter⁸, P. Riedler⁴⁰, W. Riegler⁴⁰, F. Riggi²³, A. Rivetti¹⁰², M. Rodriguez Cahuantzi⁸⁴, K. Røed⁹, D. Röhrich^{40xxx}, S. Román López⁸⁴, R. Romita^{5iv}, F. Ronchetti³⁸, P. Rosinsky⁴⁰, P. Rosnet²⁶, S. Rossegger⁴⁰, A. Rossi¹⁰³, F. Roukoutakis^{40xxxii}, S. Rousseau⁷⁷, C. Roy^{73xii}, P. Roy⁵⁴, A.J. Rubio-Montero⁶³, R. Rui¹⁰³, I. Rusanov⁴⁴, G. Russo⁹⁰, E. Ryabinkin⁷⁰, A. Rybicki²⁹, S. Sadovsky⁸³, K. Šafařík⁴⁰, R. Sahoo⁷⁹, J. Saini⁵⁵, P. Saiz⁴⁰, D. Sakata¹⁰⁵, C.A. Salgado⁹², R. Salgueiro Dominques da Silva⁴⁰, S. Salur¹⁰, T. Samanta⁵⁵, S. Sambyal⁴⁸, V. Samsonov³⁹, L. Šándor⁵⁸, A. Sandoval⁶⁶, M. Sano¹⁰⁵, S. Sano¹⁰⁰, R. Santo⁷², R. Santoro⁵, J. Sarkamo⁴⁹, P. Saturnini²⁶, E. Scapparone¹⁴, F. Scarlassara⁷⁹, R.P. Scharenberg¹⁰⁹, C. Schiaua¹⁷, R. Schicker⁴⁴, H. Schindler⁴⁰, C. Schmidt³², H.R. Schmidt³², S. Schreiner⁴⁰, S. Schuchmann³⁷, J. Schukraft⁴⁰, Y. Schutz⁷³, K. Schwarz³², K. Schweda⁴⁴, G. Scioli¹³, E. Scomparin¹⁰², G. Segato⁷⁹, D. Semenov⁹⁸, S. Senyukov¹, J. Seo⁵⁰, S. Serci¹⁹, L. Serkin⁶⁵, E. Serradilla⁶³, A. Sevcenco¹⁶, I. Sgura⁵, G. Shabratova³⁵, R. Shahoyan⁴⁰, G. Sharkov⁶⁸, N. Sharma²⁵, S. Sharma⁴⁸, K. Shigaki⁴⁵, M. Shimomura¹⁰⁵, K. Shtejer⁴², Y. Sibiriak⁷⁰, M. Siciliano¹⁰¹, E. Sicking^{40xxxiii}, E. Siddi²⁰, T. Siemiarczuk¹⁰⁷, A. Silenzi¹³, D. Silvermyr⁷⁶, E. Simili¹⁰⁶, G. Simonetti^{5x}, R. Singaraju⁵⁵, R. Singh⁴⁸, V. Singhal⁵⁵, B.C. Sinha⁵⁵, T. Sinha⁵⁴, B. Sitar¹⁵, M. Sitta¹, T.B. Skaali⁷⁸, K. Skjerdal⁸, R. Smakal⁸¹, N. Smirnov⁷⁴, R. Snellings³, H. Snow¹², C. Søgaaard²⁸, O. Sokolov⁶⁵, A. Soloviev⁸³, H.K. Soltveit⁴⁴, R. Soltz⁶⁰, W. Sommer³⁷, C.W. Son⁸⁵, H.S. Son⁹⁵, M. Song⁹⁶, C. Soos⁴⁰, F. Soramel⁷⁹, D. Soyk³², M. Spyropoulou-Stassinaki⁴, B.K. Srivastava¹⁰⁹, J. Stachel⁴⁴, F. Staley⁸⁹, I. Stan¹⁶, G. Stefanek¹⁰⁷, G. Stefanini⁴⁰, T. Steinbeck⁴³ⁱⁱ, E. Stenlund⁶¹, G. Steyn²², D. Stocco^{101xxxiv}, R. Stock³⁷, P. Stolpovsky⁸³, P. Strmen¹⁵, A.A.P. Suaide⁹³, M.A. Subieta Vásquez¹⁰¹, T. Sugitate⁴⁵, C. Suire⁷⁷, M. Šumbera⁸⁶, T. Susa¹¹³, D. Swoboda⁴⁰, J. Symons¹⁰, A. Szanto de Toledo⁹³, I. Szarka¹⁵, A. Szostak²⁰, M. Szuba¹⁰⁸, M. Tadel⁴⁰, C. Tagridis⁴, A. Takahara¹⁰⁰, J. Takahashi²¹, R. Tanabe¹⁰⁵, J.D. Tapia Takaki⁷⁷, H. Taureg⁴⁰, A. Tauro⁴⁰, M. Tavlet⁴⁰, G. Tejada Muñoz⁸⁴, A. Telesca⁴⁰, C. Terrevoli⁵, J. Thäder⁴³ⁱⁱ, R. Tieulent⁶², D. Tlustý⁸¹, A. Toia⁴⁰, T. Tolyhy¹⁸, C. Torcato de Matos⁴⁰, H. Torii⁴⁵, G. Torralba⁴³, L. Toscano¹⁰², F. Tosello¹⁰², A. Tournaire^{73xxxv}, T. Traczyk¹⁰⁸, P. Tribedy⁵⁵, G. Tröger⁴³, D. Truesdale²⁷, W.H. Trzaska⁴⁹, G. Tsileidakis⁴⁴, E. Tsilis⁴, T. Tsuji¹⁰⁰, A. Tumkin⁹⁴, R. Turrisi⁸⁰, A. Turvey³⁰, T.S. Tveter⁷⁸, H. Tydesjö⁴⁰, K. Tywoniuk⁷⁸, J. Ulery³⁷, K. Ullaland⁸, A. Uras¹⁹, J. Urbán⁵⁷, G.M. Urciuoli⁸⁸, G.L. Usai¹⁹, A. Vacchi¹⁰⁴, M. Vala^{35ix}, L. Valencia Palomo⁶⁶, S. Vallero⁴⁴, A. van den Brink¹⁰⁶, N. van der Kolk³, P. Vande Vyvre⁴⁰, M. van Leeuwen¹⁰⁶, L. Vannucci⁵⁹, A. Vargas⁸⁴, R. Varma⁷¹, A. Vasiliev⁷⁰, I. Vassiliev^{43xxxii}, M. Vassiliou⁴, V. Vechernin⁹⁸, M. Venaruzzo¹⁰³, E. Vercellin¹⁰¹, S. Vergara⁸⁴, R. Vernet^{23xxxvi}, M. Verweij¹⁰⁶, I. Vetlitskiy⁶⁸, L. Vickovic⁹⁷, G. Viesti⁷⁹, O. Vikhlyantsev⁹⁴, Z. Vilakazi²², O. Villalobos Baillie¹², A. Vinogradov⁷⁰, L. Vinogradov⁹⁸, Y. Vinogradov⁹⁴, T. Virgili⁹⁰, Y.P. Viyogi^{11xxxvii}, A. Vodopianov³⁵, K. Voloshin⁶⁸, S. Voloshin³⁴, G. Volpe⁵, B. von Haller⁴⁰, D. Vranic³², J. Vrláková⁵⁷, B. Vulpescu²⁶, B. Wagner⁸, V. Wagner⁸¹, L. Wallet⁴⁰, R. Wan^{111xxiv}, D. Wang¹¹¹, Y. Wang⁴⁴, Y. Wang¹¹¹, K. Watanabe¹⁰⁵, Q. Wen⁷, J. Wessels⁷², R. Wheadon¹⁰², J. Wiechula⁴⁴, J. Wikne⁷⁸, A. Wilk⁷², G. Wilk¹⁰⁷, M.C.S. Williams¹⁴, N. Willis⁷⁷, B. Windelband⁴⁴, C. Xu¹¹¹, C. Yang¹¹¹, H. Yang⁴⁴, A. Yasnopolsky⁷⁰, F. Yermia⁷³, J. Yi⁸⁵, Z. Yin¹¹¹, H. Yokoyama¹⁰⁵, I-K. Yoo⁸⁵, X. Yuan^{111xxxviii}, I. Yushmanov⁷⁰, E. Zabrodin⁷⁸, B. Zagreev⁶⁸, A. Zalite³⁹, C. Zampolli^{40xxxix}, Yu. Zanevsky³⁵, Y. Zaporozhets³⁵, A. Zarochentsev⁹⁸, P. Závada⁸², H. Zbroszczyk¹⁰⁸, P. Zelnicek⁴³, A. Zenin⁸³, A. Zepeda⁶⁴, I. Zgura¹⁶, M. Zhalov³⁹, X. Zhang¹¹¹ⁱ, D. Zhou¹¹¹, S. Zhou⁷, S. Zhou⁷, J. Zhu¹¹¹, A. Zichichi^{13xxii}, A. Zinchenko³⁵, G. Zinovjev⁵², M. Zinovjev⁵², Y. Zoccarato⁶², and V. Zycháček⁸¹

Affiliation notes

ⁱ Also at ²⁶

ⁱⁱ Also at ³⁶

ⁱⁱⁱ Now at ⁸⁰

^{iv} Now at ³²

^v Now at ³⁷

^{vi} Now at ²²

^{vii} Now at ¹⁷

^{viii} Also at ⁴⁶

^{ix} Now at ⁵⁷

^x Now at ⁴⁰

^{xi} Now at ⁴⁹

^{xii} Now at ⁹⁹

^{xiii} Now at ⁶

^{xiv} Now at ⁷²

^{xv} Now at: University of Technology and Austrian Academy of Sciences, Vienna, Austria

^{xvi} Also at ⁶⁰

^{xvii} Also at ⁴⁰

^{xviii} Now at: Sección Física, Departamentode de Ciencias, Pontificia Universidad Católica del Perú, Lima, Peru

^{xix} Deceased

- xx Now at⁷⁴
- xxi Now at¹⁰⁵
- xxii Also at: Centro Fermi – Centro Studi e Ricerche e Museo Storico della Fisica “Enrico Fermi”, Rome, Italy
- xxiii Now at⁵
- xxiv Also at⁴¹
- xxv Now at¹⁰¹
- xxvi Now at³⁰
- xxvii Now at⁸⁹
- xxviii Also at⁷⁸
- xxix Now at⁴⁴
- xxx Now at³³
- xxxi Now at⁸
- xxxii Now at⁴
- xxxiii Also at⁷²
- xxxiv Now at⁷³
- xxxv Now at⁶²
- xxxvi Now at: Centre de Calcul IN2P3, Lyon, France
- xxxvii Now at⁵⁵
- xxxviii Also at⁷⁹
- xxxix Also at¹⁴

Collaboration institutes

- ¹ Dipartimento di Scienze e Tecnologie Avanzate dell’Università del Piemonte Orientale and Gruppo Collegato INFN, Alessandria, Italy
- ² Department of Physics Aligarh Muslim University, Aligarh, India
- ³ National Institute for Nuclear and High Energy Physics (NIKHEF), Amsterdam, Netherlands
- ⁴ Physics Department, University of Athens, Athens, Greece
- ⁵ Dipartimento Interateneo di Fisica ‘M. Merlin’ and Sezione INFN, Bari, Italy
- ⁶ Sezione INFN, Bari, Italy
- ⁷ China Institute of Atomic Energy, Beijing, China
- ⁸ Department of Physics and Technology, University of Bergen, Bergen, Norway
- ⁹ Faculty of Engineering, Bergen University College, Bergen, Norway
- ¹⁰ Lawrence Berkeley National Laboratory, Berkeley, California, United States
- ¹¹ Institute of Physics, Bhubaneswar, India
- ¹² School of Physics and Astronomy, University of Birmingham, Birmingham, United Kingdom
- ¹³ Dipartimento di Fisica dell’Università and Sezione INFN, Bologna, Italy
- ¹⁴ Sezione INFN, Bologna, Italy
- ¹⁵ Faculty of Mathematics, Physics and Informatics, Comenius University, Bratislava, Slovakia
- ¹⁶ Institute of Space Sciences (ISS), Bucharest, Romania
- ¹⁷ National Institute for Physics and Nuclear Engineering, Bucharest, Romania
- ¹⁸ KFKI Research Institute for Particle and Nuclear Physics, Hungarian Academy of Sciences, Budapest, Hungary
- ¹⁹ Dipartimento di Fisica dell’Università and Sezione INFN, Cagliari, Italy
- ²⁰ Sezione INFN, Cagliari, Italy
- ²¹ Universidade Estadual de Campinas (UNICAMP), Campinas, Brazil
- ²² Physics Department, University of Cape Town, iThemba Laboratories, Cape Town, South Africa
- ²³ Dipartimento di Fisica e Astronomia dell’Università and Sezione INFN, Catania, Italy
- ²⁴ Sezione INFN, Catania, Italy
- ²⁵ Physics Department, Panjab University, Chandigarh, India
- ²⁶ Laboratoire de Physique Corpusculaire (LPC), Clermont Université, Université Blaise Pascal, CNRS-IN2P3, Clermont-Ferrand, France
- ²⁷ Department of Physics, Ohio State University, Columbus, Ohio, United States
- ²⁸ Niels Bohr Institute, University of Copenhagen, Copenhagen, Denmark
- ²⁹ The Henryk Niewodniczanski Institute of Nuclear Physics, Polish Academy of Sciences, Cracow, Poland
- ³⁰ Physics Department, Creighton University, Omaha, Nebraska, United States
- ³¹ Universidad Autónoma de Sinaloa, Culiacán, Mexico
- ³² ExtreMe Matter Institute EMMI, GSI Helmholtzzentrum für Schwerionenforschung, Darmstadt, Germany
- ³³ Institut für Kernphysik, Technische Universität Darmstadt, Darmstadt, Germany
- ³⁴ Wayne State University, Detroit, Michigan, United States
- ³⁵ Joint Institute for Nuclear Research (JINR), Dubna, Russia

- 36 Frankfurt Institute for Advanced Studies, Johann Wolfgang Goethe-Universität Frankfurt, Frankfurt, Germany
37 Institut für Kernphysik, Johann Wolfgang Goethe-Universität Frankfurt, Frankfurt, Germany
38 Laboratori Nazionali di Frascati, INFN, Frascati, Italy
39 Petersburg Nuclear Physics Institute, Gatchina, Russia
40 European Organization for Nuclear Research (CERN), Geneva, Switzerland
41 Laboratoire de Physique Subatomique et de Cosmologie (LPSC), Université Joseph Fourier, CNRS-IN2P3, Institut Polytechnique de Grenoble, Grenoble, France
42 Centro de Aplicaciones Tecnológicas y Desarrollo Nuclear (CEADEN), Havana, Cuba
43 Kirchoff-Institut für Physik, Ruprecht-Karls-Universität Heidelberg, Heidelberg, Germany
44 Physikalisches Institut, Ruprecht-Karls-Universität Heidelberg, Heidelberg, Germany
45 Hiroshima University, Hiroshima, Japan
46 University of Houston, Houston, Texas, United States
47 Physics Department, University of Rajasthan, Jaipur, India
48 Physics Department, University of Jammu, Jammu, India
49 Helsinki Institute of Physics (HIP) and University of Jyväskylä, Jyväskylä, Finland
50 Kangnung National University, Kangnung, South Korea
51 Scientific Research Technological Institute of Instrument Engineering, Kharkov, Ukraine
52 Bogolyubov Institute for Theoretical Physics, Kiev, Ukraine
53 University of Tennessee, Knoxville, Tennessee, United States
54 Saha Institute of Nuclear Physics, Kolkata, India
55 Variable Energy Cyclotron Centre, Kolkata, India
56 Fachhochschule Köln, Köln, Germany
57 Faculty of Science, P.J. Šafárik University, Košice, Slovakia
58 Institute of Experimental Physics, Slovak Academy of Sciences, Košice, Slovakia
59 Laboratori Nazionali di Legnaro, INFN, Legnaro, Italy
60 Lawrence Livermore National Laboratory, Livermore, California, United States
61 Division of Experimental High Energy Physics, University of Lund, Lund, Sweden
62 Université de Lyon 1, CNRS/IN2P3, Institut de Physique Nucléaire de Lyon, Lyon, France
63 Centro de Investigaciones Energéticas Medioambientales y Tecnológicas (CIEMAT), Madrid, Spain
64 Centro de Investigación y de Estudios Avanzados (CINVESTAV), Mexico City and Mérida, Mexico
65 Instituto de Ciencias Nucleares, Universidad Nacional Autónoma de México, Mexico City, Mexico
66 Instituto de Física, Universidad Nacional Autónoma de México, Mexico City, Mexico
67 Institute for Nuclear Research, Academy of Sciences, Moscow, Russia
68 Institute for Theoretical and Experimental Physics, Moscow, Russia
69 Moscow Engineering Physics Institute, Moscow, Russia
70 Russian Research Centre Kurchatov Institute, Moscow, Russia
71 Indian Institute of Technology, Mumbai, India
72 Institut für Kernphysik, Westfälische Wilhelms-Universität Münster, Münster, Germany
73 SUBATECH, Ecole des Mines de Nantes, Université de Nantes, CNRS-IN2P3, Nantes, France
74 Yale University, New Haven, Connecticut, United States
75 Budker Institute for Nuclear Physics, Novosibirsk, Russia
76 Oak Ridge National Laboratory, Oak Ridge, Tennessee, United States
77 Institut de Physique Nucléaire d'Orsay (IPNO), Université Paris-Sud, CNRS-IN2P3, Orsay, France
78 Department of Physics, University of Oslo, Oslo, Norway
79 Dipartimento di Fisica dell'Università and Sezione INFN, Padova, Italy
80 Sezione INFN, Padova, Italy
81 Faculty of Nuclear Sciences and Physical Engineering, Czech Technical University in Prague, Prague, Czech Republic
82 Institute of Physics, Academy of Sciences of the Czech Republic, Prague, Czech Republic
83 Institute for High Energy Physics, Protvino, Russia
84 Benemérita Universidad Autónoma de Puebla, Puebla, Mexico
85 Pusan National University, Pusan, South Korea
86 Nuclear Physics Institute, Academy of Sciences of the Czech Republic, Řež u Prahy, Czech Republic
87 Dipartimento di Fisica dell'Università 'La Sapienza' and Sezione INFN, Rome, Italy
88 Sezione INFN, Rome, Italy
89 Commissariat à l'Energie Atomique, IRFU, Saclay, France
90 Dipartimento di Fisica 'E.R. Caianiello' dell'Università and Sezione INFN, Salerno, Italy
91 California Polytechnic State University, San Luis Obispo, California, United States
92 Departamento de Física de Partículas and IGFAE, Universidad de Santiago de Compostela, Santiago de Compostela, Spain
93 Universidade de São Paulo (USP), São Paulo, Brazil
94 Russian Federal Nuclear Center (VNIIEF), Sarov, Russia
95 Department of Physics, Sejong University, Seoul, South Korea
96 Yonsei University, Seoul, South Korea

- ⁹⁷ Technical University of Split FESB, Split, Croatia
⁹⁸ V. Fock Institute for Physics, St.Petersburg State University, St.Petersburg, Russia
⁹⁹ Institut Pluridisciplinaire Hubert Curien (IPHC), Université de Strasbourg, CNRS-IN2P3, Strasbourg, France
¹⁰⁰ University of Tokyo, Tokyo, Japan
¹⁰¹ Dipartimento di Fisica Sperimentale dell'Università and Sezione INFN, Turin, Italy
¹⁰² Sezione INFN, Turin, Italy
¹⁰³ Dipartimento di Fisica dell'Università and Sezione INFN, Trieste, Italy
¹⁰⁴ Sezione INFN, Trieste, Italy
¹⁰⁵ University of Tsukuba, Tsukuba, Japan
¹⁰⁶ Institute for Subatomic Physics, Utrecht University, Utrecht, Netherlands
¹⁰⁷ Soltan Institute for Nuclear Studies, Warsaw, Poland
¹⁰⁸ Warsaw University of Technology, Warsaw, Poland
¹⁰⁹ Purdue University, West Lafayette, Indiana, United States
¹¹⁰ Zentrum für Technologietransfer und Telekommunikation (ZTT), Fachhochschule Worms, Worms, Germany
¹¹¹ Hua-Zhong Normal University, Wuhan, China
¹¹² Yerevan Physics Institute, Yerevan, Armenia
¹¹³ Rudjer Bošković Institute, Zagreb, Croatia

Abstract. On 23rd November 2009, during the early commissioning of the CERN Large Hadron Collider (LHC), two counter-rotating proton bunches were circulated for the first time concurrently in the machine, at the LHC injection energy of 450 GeV per beam. Although the proton intensity was very low, with only one pilot bunch per beam, and no systematic attempt was made to optimize the collision optics, all LHC experiments reported a number of collision candidates. In the ALICE experiment, the collision region was centred very well in both the longitudinal and transverse directions and 284 events were recorded in coincidence with the two passing proton bunches. The events were immediately reconstructed and analyzed both online and offline. We have used these events to measure the pseudorapidity density of charged primary particles in the central region. In the range $|\eta| < 0.5$, we obtain $dN_{\text{ch}}/d\eta = 3.10 \pm 0.13(\text{stat.}) \pm 0.22(\text{syst.})$ for all inelastic interactions, and $dN_{\text{ch}}/d\eta = 3.51 \pm 0.15(\text{stat.}) \pm 0.25(\text{syst.})$ for non-single diffractive interactions. These results are consistent with previous measurements in proton–antiproton interactions at the same centre-of-mass energy at the CERN Sp \bar{p} S collider. They also illustrate the excellent functioning and rapid progress of the LHC accelerator, and of both the hardware and software of the ALICE experiment, in this early start-up phase.

1 Introduction

The very first proton–proton collisions at Point 2 of the CERN Large Hadron Collider (LHC) [1] occurred in the afternoon of 23rd November 2009, at a centre-of-mass energy $\sqrt{s} = 900$ GeV, during the commissioning of the accelerator. This publication, based on 284 events recorded in the ALICE detector [2] on that day, describes a determination of the pseudorapidity density of charged primary particles¹ $dN_{\text{ch}}/d\eta$ ($\eta \equiv -\ln \tan \theta/2$, where θ is the polar angle with respect to the beam line) in the central pseudorapidity region. The purpose of this study is to compare with previous measurements for proton–antiproton ($p\bar{p}$) collisions at the same energy [3], and to establish a reference for comparison with forthcoming measurements at higher LHC energies.

The event sample collected with our trigger contains three different classes of inelastic interactions, i.e. collisions where new particles are produced: non-diffractive, single-diffractive, and double-diffractive². Experimentally

¹ Here, primary particles are defined as prompt particles produced in the collision and all decay products, except products from weak decays of strange particles such as K_s^0 and Λ .

² Inelastic pp collisions are usually divided into these classes depending on the fate of the interacting protons. If one (both)

we cannot distinguish between these classes, which, however, are selected by our trigger with different efficiencies³.

In order to compare our data with those of other experiments, we provide the result with two different normalizations: the first one (INEL) corresponds to the sum of all inelastic interactions and corrects the trigger bias individually for all event classes, by weighting them, each with its own estimated trigger efficiency and abundance. The second normalization (non-single-diffractive or NSD) applies this correction for non-diffractive and double-diffractive processes only, while removing, on average, the single-diffractive contribution.

Multiparticle production is rather successfully described by phenomenological models with Pomeron exchange, which dominates at high energies [4, 5]. These models re-

incoming beam particle(s) are excited into a high-mass state, the process is called single (double) diffraction; otherwise the events are classified as non-diffractive. Particles emitted in diffractive reactions are usually found at rapidities close to that of the parent proton.

³ We estimate the *trigger efficiency* for each class using the process-type information provided by Monte Carlo generators; the values vary by up to a factor of two between classes and are listed in Section 3. The *relative abundance* of each class is taken from published data (see text).

late the energy dependence of the total cross section to that of the multiplicity production using a small number of parameters, and are the basis for several Monte Carlo event generators describing soft hadron collisions (see for example [6–8]). According to these models, it is expected that the charged-particle density increases by a factor 1.7 and 1.9 when raising the LHC centre-of-mass energy from 900 GeV to 7 and 14 TeV respectively (i.e. intermediate and nominal LHC energies). The difference in charged-particle densities between $p\bar{p}$ and pp interactions is predicted to decrease as $1/\sqrt{s}$ at high energies [9]. This difference was last measured at the CERN ISR to be in the range 1.5–3% [10] at $\sqrt{s} = 53$ GeV. Extrapolating these values to $\sqrt{s} = 900$ GeV, one obtains a very small difference of about 0.1–0.2%. Therefore, we will compare our measurement to existing $p\bar{p}$ data and also to different Monte Carlo models.

This article is organized as follows: Section 2 describes the experimental conditions during data taking; the main features of the ALICE detector subsystems used for this analysis are described in Section 3; Section 4 is dedicated to the event selection and data analysis; the results are discussed in Section 5 and Section 6 contains the conclusion.

2 LHC and the run conditions

The LHC, built at CERN in the circular tunnel of 27 km circumference previously used by the Large Electron–Positron collider (LEP), will provide the highest energy ever explored with particle accelerators. It is designed to collide two counter-rotating beams of protons or heavy ions. The nominal centre-of-mass energy for proton–proton collisions is 14 TeV. However, collisions can be obtained down to $\sqrt{s} = 900$ GeV, which corresponds to the beam injection energy.

The results from the first proton–proton collisions presented here were obtained during the early commissioning phase of the LHC, when two proton bunches were circulating for the first time concurrently in the machine. The bunches used were the so-called “pilot bunches”: low intensity bunches used during machine commissioning, with a few 10^9 protons per bunch. The two beams were brought into nominal position for collisions without a specific attempt to maximize the interaction rate. The nominal r.m.s. size of LHC beams at injection energy is about $300 \mu\text{m}$ in the transverse direction and 10.5 cm in the longitudinal (z -axis) direction. However, at this early stage, the beam parameters can deviate from these nominal values; they were not measured for the fill used in this analysis. For the previous fill, for which the longitudinal size was measured, it was found to be shorter, with an r.m.s. of about 8 cm. Assuming Gaussian beam profiles, the luminous region should be smaller than the beam size by a factor of $\sqrt{2}$ in all directions.

Shortly after circulating beams were established, the ALICE data acquisition system [11] started collecting events with a trigger based on the Silicon Pixel Detector

(SPD), requiring two or more hits in the SPD in coincidence with the passage of the two colliding bunches as inferred from beam pickup detectors. As a precaution, only a small subset of the detector subsystems, including the silicon tracking detectors and the scintillator trigger counters, was turned on, in order to assess the beam conditions provided by the LHC.

The trigger rate was measured just before collisions with the same trigger conditions. Without beams we measured a rate of 3×10^{-4} Hz (in coincidence with one bunch crossing interval per orbit). In coincidence with the passage of the bunch of one circulating beam the rate was 0.006 Hz. As soon as the second beam was injected in the accelerator, the event rate increased significantly, to 0.11 Hz. The first event that was analyzed and displayed in the counting room by the offline reconstruction software AliRoot [12] running in online mode is shown in Fig. 1. This marked symbolically the keenly anticipated start of the physics exploitation of the ALICE experiment⁴. The online reconstruction software implemented in the High-Level Trigger (HLT) computer farm [13] also analyzed the events in real time and calculated the vertex position of the collected events, shown in Fig. 2. The distributions are very narrow in the transverse plane (sub-millimetre, including contributions from detector resolution and residual misalignment), of about the expected size in the longitudinal direction and well positioned with respect to the nominal centre of the ALICE detector. This provided immediate evidence that a substantial fraction of the events corresponded to collisions between the protons of the two counter-rotating beams.

After 43 minutes, the two beams were dumped in order to proceed with the LHC commissioning programme. In total, 284 events were triggered and recorded during this short, but important, first run of the ALICE experiment with colliding beams.

3 The ALICE experiment

ALICE, designed as the dedicated heavy-ion experiment at the LHC, also has excellent performance for proton–proton interactions [14]. The experiment consists of a large number of detector subsystems [2] inside a solenoidal magnet ($B = 0.5$ T). The magnet was off during this run.

During the several months of running with cosmic rays in 2008 and 2009, all of the ALICE detector subsystems were extensively commissioned, calibrated and used for data taking [15]. Data were collected for an initial alignment of the parts of the detector that had sufficient exposure to the mostly vertical cosmic ray flux. Data were also taken during various LHC injection tests to perform timing measurements and other calibrations.

Collisions take place at the centre of the ALICE detector, inside a beryllium vacuum beam pipe (3 cm in radius and $800 \mu\text{m}$ thick). The tracking system in the ALICE central barrel covers the full azimuthal range in the

⁴ The event display started shortly after data taking and therefore missed the first few events.

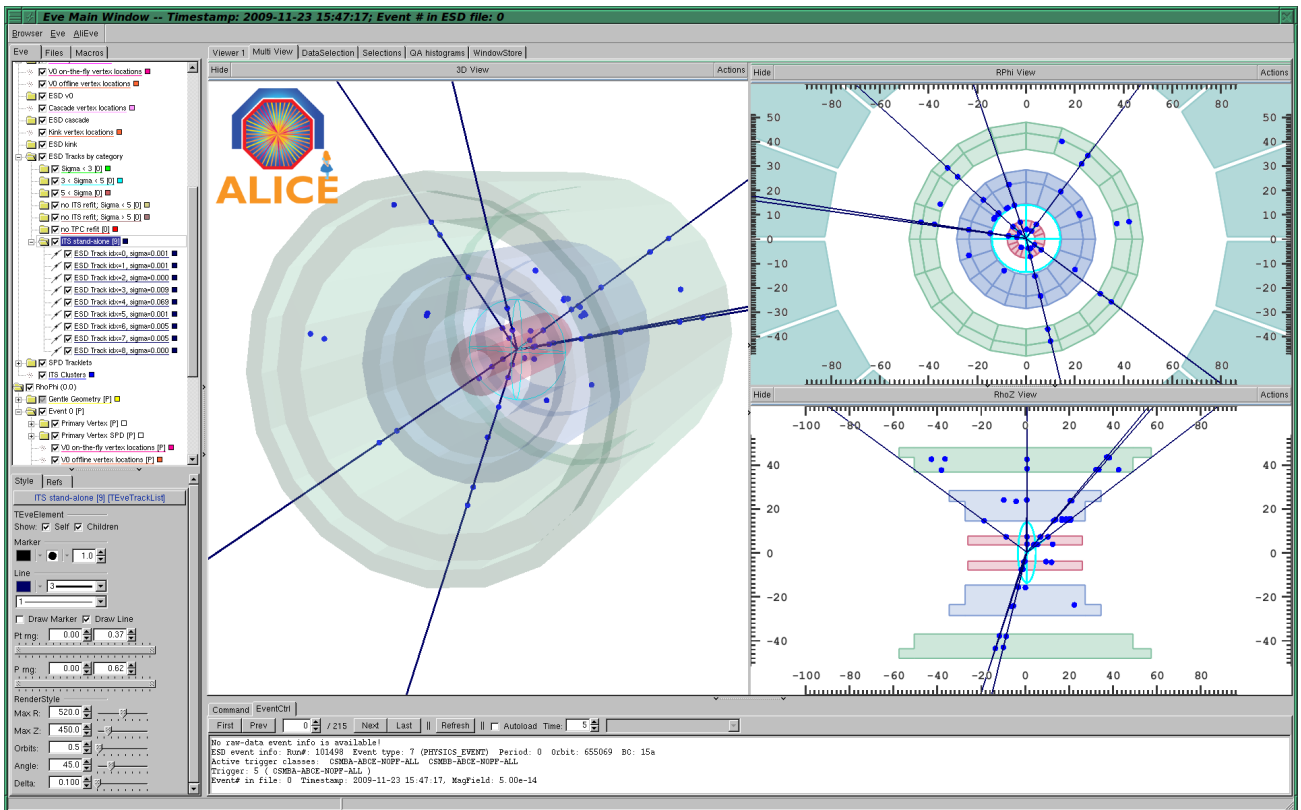


Fig. 1. The first pp collision candidate shown by the event display in the ALICE counting room (3D view, r - ϕ and r - z projections), the dimensions are shown in cm. The dots correspond to hits in the silicon vertex detectors (SPD, SDD and SSD), the lines correspond to tracks reconstructed using loose quality cuts. The ellipse drawn in the middle of the detector surrounds the reconstructed event vertex.

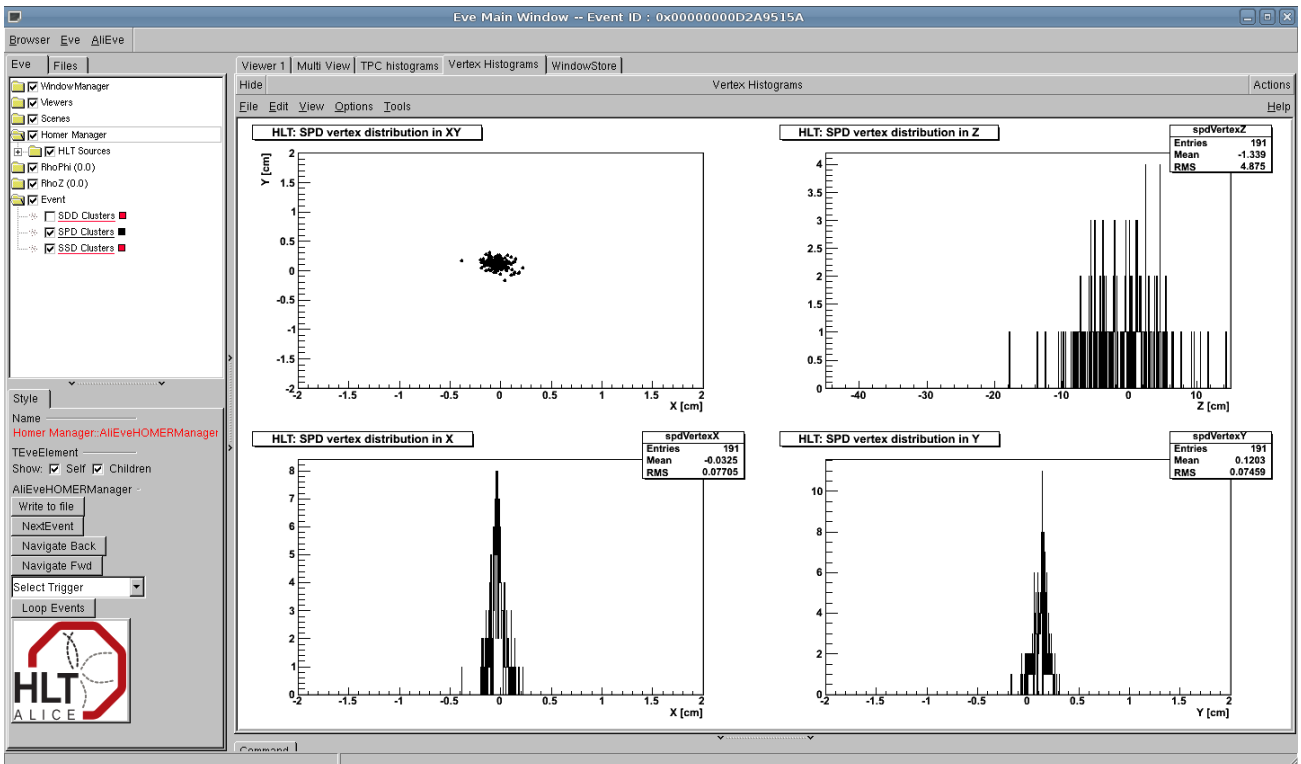


Fig. 2. Online display of the vertex positions reconstructed by the High-Level Trigger (HLT). The figure shows, counter-clockwise from top left, the position in the transverse plane for all events with a reconstructed vertex, the projections along the transverse coordinates x and y , and the distribution along the beam line (z -axis).

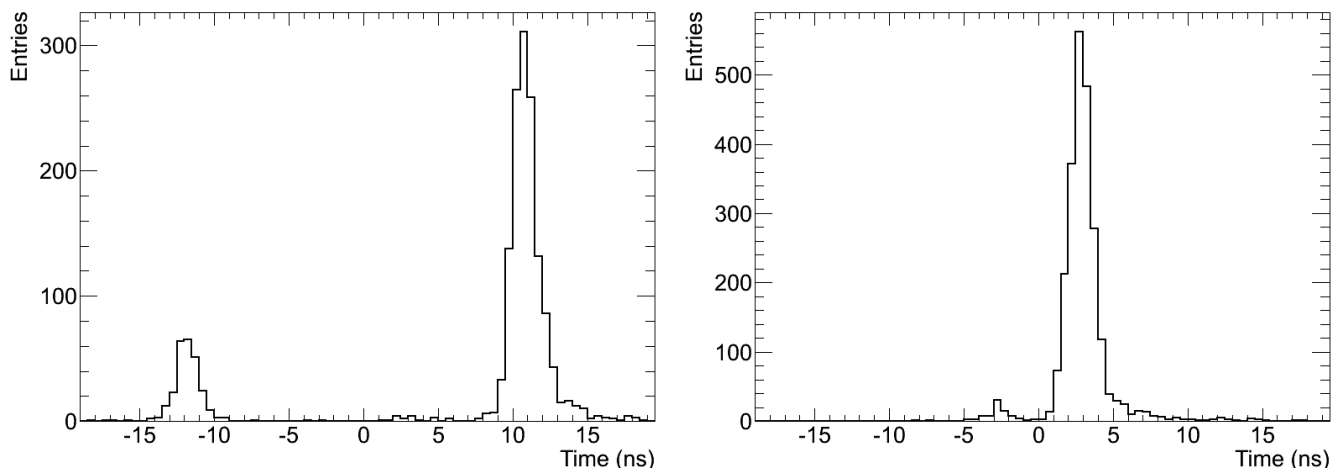


Fig. 3. Arrival time of particles in the VZERO detectors relative to the beam crossing time (time zero). A number of beam-halo or beam-gas events are visible as secondary peaks in VZERO-A (left panel) and VZERO-C (right panel). This is because particles produced in background interactions arrive at earlier times in one or the other of the two counters. The majority of the signals have the correct arrival time expected for collisions around the nominal vertex.

pseudorapidity window $|\eta| < 0.9$. It has been designed to cope with the highest charged-particle densities expected in central Pb–Pb collisions. The following four detector subsystems were active during data taking and were used in this analysis.

- The Silicon Pixel Detector (SPD) consists of two cylindrical layers with radii of 3.9 and 7.6 cm and has about 9.8 million pixels of size $50 \times 425 \mu\text{m}^2$. It covers the pseudorapidity ranges $|\eta| < 2$ and $|\eta| < 1.4$ for the inner and outer layers respectively, for particles originating at the centre of the detector. The effective η -acceptance is larger due to the longitudinal spread of the position of the interaction vertex. The detector is read out by custom-designed ASICs bump-bonded directly on silicon ladders. Each chip contains 8192 channels and also provides a fast trigger signal if at least one of its pixels is hit. The trigger signals from all 1200 chips are then combined in a programmable logic unit which provides a level-0 trigger signal to the central trigger processor. The total thickness of the SPD amounts to about 2.3% of a radiation length. About 83% of the channels were operational for particle detection and 77% of the chips were used in the trigger logic. The SPD was aligned using cosmic-ray tracks collected during 2008 [16], and the residual misalignment was estimated to be below $10 \mu\text{m}$ for the modules well covered by mostly vertical tracks. The modules on the sides are likely to be affected by larger residual misalignment.
- The Silicon Drift Detector (SDD) consists of two cylindrical layers at radii of 15.0 and 23.9 cm and covers the region $|\eta| < 0.9$. It is composed of 260 sensors with an internal voltage divider providing a drift field of 500 V/cm and MOS charge injectors that allow measurement of the drift speed via dedicated calibration triggers. The charge signal of each of the 133 000 collection anodes, arranged with a pitch of $294 \mu\text{m}$,

is sampled every 50 ns by an ADC in the front-end electronics. The total thickness of the SDD layers (including mechanical supports and front-end electronics) amounts to 2.4% of a radiation length. About 92% of the anodes were fully operational.

- The two layers of the double-sided Silicon Strip Detector (SSD) are located at radii of 38 and 43 cm respectively, covering $|\eta| < 0.97$. The SSD consists of 1698 sensors with a strip pitch of $95 \mu\text{m}$ and a stereo angle of 35 mrad. The detector provides a measurement of the charge deposited in each of its 2.5×10^6 strips. The position resolution is better than $20 \mu\text{m}$ in the r - φ direction and about 0.8 mm in the direction along the beam line. The thickness of the SSD, including supports and services, corresponds to 2.2% of a radiation length. About 90% of the SSD area was active during data taking.
- The VZERO detector consists of two arrays of 32 scintillators each, which are placed around the beam pipe on either side of the interaction region: VZERO-A at $z = 3.3$ m, covering the pseudorapidity range $2.8 < \eta < 5.1$, and VZERO-C at $z = -0.9$ m, covering the pseudorapidity range $-3.7 < \eta < -1.7$. The time resolution of this detector is better than 1 ns. Its response is recorded in a time window of ± 25 nsec around the nominal beam crossing time. For events collected in this run, the arrival times of particles at the detector relative to this “time zero” is shown in Fig. 3. Note that in general several particles are registered for each event. Particles hitting one of the detectors before the beam crossing have negative arrival times and are typically due to interactions taking place outside the central region of ALICE.

More details about the ALICE experiment and its detector subsystems can be found in [2].

The trigger used to record the events for the present analysis is defined by requiring at least two hit chips in

the SPD, in coincidence with the signals from the two beam pick-up counters indicating the presence of two passing proton bunches. The efficiency of this trigger as well as all other corrections have been studied using two different Monte Carlo generators, PYTHIA 6.4.14 [17] tune D6T [18] and PHOJET [8], for INEL and NSD interactions. The trigger efficiencies for non-diffractive, single-diffractive, and double-diffractive events were evaluated separately, and found to be 98–99 %, 48–58 %, and 53–76 % respectively. The ranges are determined by the two event generators. These event classes were combined for the corrections using the fractions measured by UA5 [19]: non-diffractive 0.767 ± 0.059 ; single-diffractive 0.153 ± 0.031 ; double-diffractive 0.08 ± 0.05 . The resulting efficiencies were found to be 87–91 % for the INEL normalization and 94–97 % for the NSD normalization, again depending on the event generator used.

The results presented in the following sections are those obtained with PYTHIA. The difference between results corrected with PYTHIA and PHOJET is used in the estimate of the systematic uncertainty.

4 Data analysis

The data sample used in the present analysis consists of 284 events recorded without magnetic field. The results presented here are based on the analysis of the SPD data. However, information from the SDD, SSD and VZERO was used to crosscheck the identification and removal of background events.

In the SPD analysis, the position of the interaction vertex is reconstructed [20] by correlating hits in the two silicon-pixel layers to obtain tracklets. The achieved resolution depends on the track multiplicity and for this specific vertex reconstruction is approximately 0.1–0.3 mm in the longitudinal direction and 0.2–0.5 mm in the transverse direction. For events with only one charged track, the vertex position is determined by intersecting the SPD tracklet with the mean beam axis determined from the vertex positions of other events in the sample. A vertex was reconstructed in 94 % of the selected events. The distribution of the vertex position in the longitudinal direction (z -axis) is shown in Fig. 4. For events originating from the centre of the detector, the vertex-reconstruction efficiency was estimated, using Monte Carlo simulations, to be 84 % for INEL interactions and 92 % for NSD collisions. These efficiencies decrease for larger $|z|$ -values of the vertex in low-multiplicity events; therefore, only events with vertices within $|z| < 10$ cm were used. This allows for an accurate charged-particle density measurement in the pseudorapidity range $|\eta| < 1.6$ using both SPD layers.

Using the reconstructed vertex as the origin, we calculate the differences in azimuthal ($\Delta\varphi$, bending plane) and polar ($\Delta\theta$, non-bending direction) angles of pairs of hits with one hit in each SPD layer. These tracklets [21] are selected by a cut on the sum of the squares of $\Delta\varphi$ and $\Delta\theta$, each normalized to its estimated resolution (80 mrad and 25 mrad, respectively). When more than one hit in a layer matches a hit in the other layer, only the hit combination

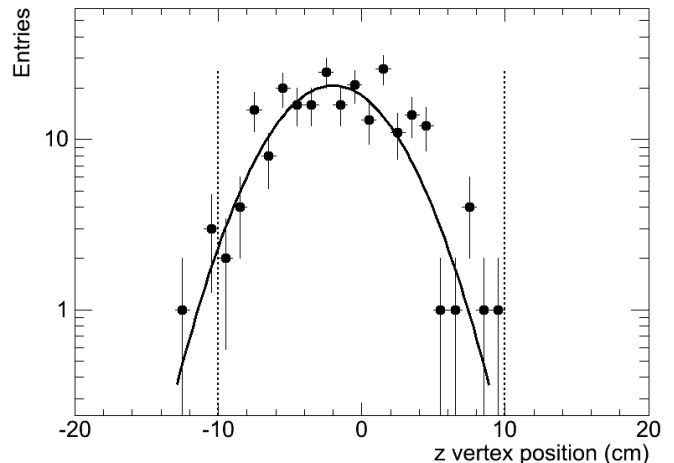


Fig. 4. Longitudinal vertex distribution from hit correlations in the two pixel layers of the ALICE inner tracking system. Vertical dashed lines indicate the region $|z| < 10$ cm, where the events for the present analysis are selected. A Gaussian fit with an estimated r.m.s. of about 4 cm to the central part is also shown.

with the smallest angular difference is used. This occurs in only 2 % of the matched hits.

The number of primary charged particles is estimated by counting the number of tracklets. This number was corrected for:

- trigger inefficiency;
- detector and reconstruction inefficiencies;
- contamination by decay products of long-lived particles (K_s^0 , Λ , etc.), gamma conversions and secondary interactions.

The corrections are determined as a function of the z -position of the primary vertex, and on the pseudorapidity of the tracklet. For the analyzed sample the average correction factor for tracklets is about 1.5.

The beam-gas and beam-halo background events were removed by a cut on the ratio between the number of tracklets and the total number of hits in the tracking system (SPD, SDD, and SSD); this ratio is smaller for background events (as measured in the previous fills triggering on the bunch passage from one side) than for collisions [22]. In addition, the timing information from the VZERO detector was used for background rejection by removing events with negative arrival time (see Fig. 3). The event quality and event classification was crosschecked by a visual scan of the whole event sample. In total 29 events (i.e. about 10 %) were rejected as beam induced background, which is consistent with the rate expected from previous fills. The remaining background was estimated from the vertex distribution and found to be negligible. The contamination from coincidence with a cosmic event was estimated to be one event in the full sample. Indeed, two cosmic events were identified by scanning, both without reconstructed vertex.

Particular attention has been paid to events having zero or one charged tracklets in the SPD acceptance. The

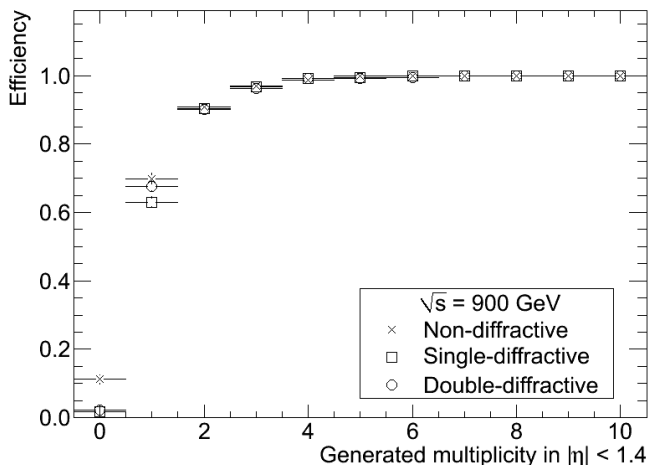


Fig. 5. Multiplicity dependence of the combined efficiency to select an event as minimum bias and to reconstruct its vertex in SPD, for non-diffractive (crosses), single-diffractive (squares), and double-diffractive (circles) events, based on PYTHIA events.

vertex-finding efficiency for events with one charged particle in the acceptance is about 80 %. The number of zero-track events has been estimated by Monte Carlo calculations. The total number of collisions used for the normalization was calculated from the number of events selected for the analysis, corrected for the vertex-reconstruction inefficiency. In order to obtain the normalization for INEL and NSD events, we further corrected the number of selected events for the trigger efficiency for these two event classes. In addition, for NSD events, we subtract the single-diffractive contribution. These corrections, as well as those for the vertex finding efficiency, depend on the event charged-particle multiplicity, see Fig. 5. The dependence of the event-finding efficiency (combining event selection and vertex finding) on multiplicity was calculated for different interaction types using our detector simulation, and is above 98 % for events with at least two charged particles. The averaged combined corrections for the vertex reconstruction efficiency and the selection efficiency is 20 % for INEL interactions and much smaller for NSD interactions, due to the cancelation of some contributions.

The various corrections mentioned above were calculated using the full GEANT 3 [23] simulation of the ALICE detector as included in the offline framework AliRoot. In order to estimate the systematic uncertainties, the above analysis was repeated by:

- applying different cuts for the tracklet definition (varying the angle cut-off by $\pm 50\%$);
- varying by $\pm 10\%$ the density of the material in the tracking system, thus changing the material budget;
- using the non-aligned geometry;
- varying by $\pm 30\%$ the composition of the produced particle types with respect to the yields suggested by the event generators;
- varying the particle yield below 100 MeV/c by $\pm 30\%$;

Table 1. Contributions to systematic uncertainties on the measurement of the charged-particle pseudorapidity density.

Uncertainty	
Tracklet selection cuts	negl.
Material budget	negl.
Misalignment	0.5 %
Particle composition	negl.
Transverse-momentum spectrum	0.5 %
Contribution of diffraction (INEL)	4 %
Contribution of diffraction (NSD)	4.5 %
Event-generator dependence (INEL)	4 %
Event-generator dependence (NSD)	3 %
Detector efficiency	4 %
SPD triggering efficiency	2 %
Background events	negl.
Total (INEL)	7.2 %
Total (NSD)	7.1 %

- evaluating the uncertainty in the normalization to INEL and NSD samples by varying the ratios of the non-diffractive, single-diffractive and double-diffractive cross sections according to their measured values and errors [19] and using two different models for diffraction kinematics (PYTHIA and PHOJET).

An additional source of systematic error comes from the limited statistics used so far to determine the efficiencies of the SPD detector modules. In test beams, the SPD efficiency in active areas was measured to be higher than 99.8 %. This was crosschecked in-situ with cosmic data, but only over a limited area and with limited statistics. At this stage, we have assigned a conservative value of 4 % to this uncertainty. The triggering efficiency of the SPD was estimated from the data itself, using the trigger information recorded in the data stream for events with more than one tracklet, and found to be very close to 100 %, with an error of about 2 % (due to the limited statistics).

These contributions to the systematic uncertainty on the charged particle pseudorapidity density are summarized in Table 1. Our conclusion is that the total systematic uncertainty on the pseudorapidity density is less than $\pm 7.2\%$ for INEL collisions and $\pm 7.1\%$ for NSD collisions. The largest contribution comes from uncertainties in cross sections of diffractive processes and their kinematic simulation.

More details about this analysis, corrections, and the evaluation of the systematic uncertainties can be found in [24].

5 Results

Figure 6 shows the charged primary particle pseudorapidity density distributions obtained for INEL and NSD interactions in the range $|\eta| < 1.6$. The pseudorapidity density obtained in the central region $|\eta| < 0.5$ for INEL interactions is $3.10 \pm 0.13(stat.) \pm 0.22(syst.)$ and for NSD interac-

Table 2. Comparison of charged primary particle pseudorapidity densities at central pseudorapidity ($|\eta| < 0.5$) for inelastic (INEL) and non-single diffractive (NSD) collisions measured by the ALICE detector in pp interactions and by UA5 in $p\bar{p}$ interactions [3] at a centre-of-mass energy of 900 GeV. For ALICE, the first error is statistical and the second is systematic; no systematic error is quoted by UA5. The experimental data are also compared to the predictions for pp collisions from different models. For PYTHIA the tune versions are given in parentheses. The correspondence is as follows: D6T is tune (109); ATLAS CSC is tune (306); Perugia-0 is tune (320).

Experiment Model	ALICE pp	UA5 $p\bar{p}$ [3]	QGSM [25]	PYTHIA [17] (109) [18] (306) [26] (320) [27]	PHOJET [8]
INEL	$3.10 \pm 0.13 \pm 0.22$	3.09 ± 0.05	2.98	2.33 2.99 2.46	3.14
NSD	$3.51 \pm 0.15 \pm 0.25$	3.43 ± 0.05	3.47	2.83 3.68 3.02	3.61

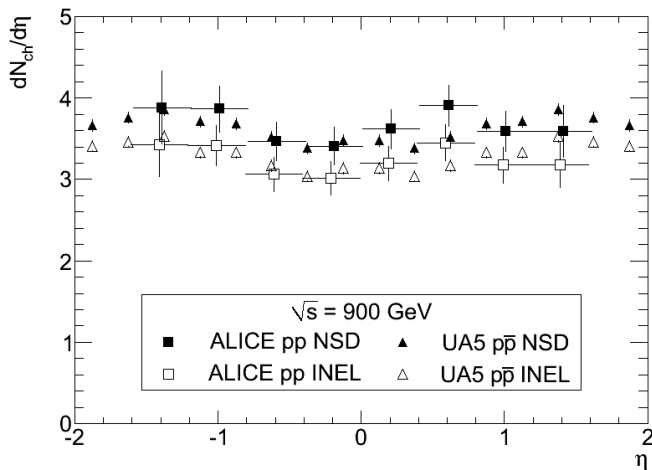


Fig. 6. Pseudorapidity dependence of $dN_{\text{ch}}/d\eta$ for INEL and NSD collisions. The ALICE measurements (squares) are compared to UA5 data (triangles) [3]. The errors shown are statistical only.

tions is $3.51 \pm 0.15(\text{stat.}) \pm 0.25(\text{sys.})$. Also shown in Fig. 6 are the previous measurements of proton–antiproton interactions from the UA5 experiment [3]. Our results obtained for proton–proton interactions are consistent with those for proton–antiproton interactions, as expected from the fact that the predicted difference (0.1–0.2%) is well below measurement uncertainties. The measurements at central pseudorapidity ($|\eta| < 0.5$) are summarized in Table 2 together with model predictions obtained with QGSM, PHOJET and three different PYTHIA tunes. PYTHIA 6.4.14, tune D6T, and PHOJET yield respectively the lowest and highest charged particle densities. Therefore, these two have been used for the evaluation of our systematic errors. PYTHIA 6.4.20, tunes ATLAS CSC and Perugia-0, are candidates for use by the LHC experiments at higher LHC energies and are shown for comparison.

Figure 7 shows the centre-of-mass energy dependence of the pseudorapidity density in the central region ($|\eta| < 0.5$). The data points are obtained in the $|\eta| < 0.5$ range from this experiment and from references [3, 10, 28–31], and are corrected for differences in pseudorapidity range where necessary, fitting the pseudorapidity distribution around $\eta = 0$. As noted above, there is good agreement between pp and $p\bar{p}$ data at the same energy. The dashed and solid

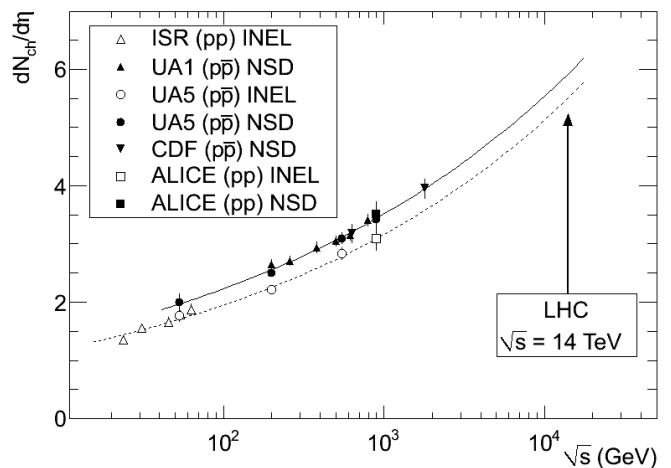


Fig. 7. Charged-particle pseudorapidity density in the central rapidity region in proton–proton and proton–antiproton interactions as a function of the centre-of-mass energy. The dashed and solid lines (for INEL and NSD interactions respectively) indicate the fit using a power-law dependence on energy.

lines (for INEL and NSD interactions respectively) are obtained by fitting the density of charged particles in the central pseudorapidity rapidity region with a power-law dependence on energy.

Using this parametrization, the extrapolation to the nominal LHC energy of $\sqrt{s} = 14$ TeV yields $dN_{\text{ch}}/d\eta = 5.5$ and $dN_{\text{ch}}/d\eta = 5.9$ for INEL and NSD interactions respectively.

6 Conclusion

Proton–proton collisions observed with the ALICE detector in the early phase of the LHC commissioning have been used to measure the pseudorapidity density of charged primary particles at $\sqrt{s} = 900$ GeV. In the central pseudorapidity region ($|\eta| < 0.5$), we obtain $dN_{\text{ch}}/d\eta = 3.10 \pm 0.13(\text{stat.}) \pm 0.22(\text{sys.})$ for all inelastic and $dN_{\text{ch}}/d\eta = 3.51 \pm 0.15(\text{stat.}) \pm 0.25(\text{sys.})$ for non-single diffractive proton–proton interactions. The results are consistent with earlier measurements of primary charged-particle production in proton–antiproton interactions at the same energy. They are also compared with model calculations.

These results have been obtained with a small sample of events during the early commissioning of the LHC. They demonstrate that the LHC and its experiments have finally entered the phase of physics exploitation, within days of starting up the accelerator complex in November 2009.

Acknowledgements

The ALICE collaboration would like to thank all its engineers and technicians for their invaluable contributions to the construction of the experiment. We would like to thank and congratulate the CERN accelerator teams for the outstanding performance of the LHC complex at start up, and for providing us with the collisions used for this paper on such a short notice!

The ALICE collaboration acknowledges the following funding agencies for their support in building and running the ALICE detector:

- Calouste Gulbenkian Foundation from Lisbon and Swiss Fonds Kidagan, Armenia;
- Conselho Nacional de Desenvolvimento Científico e Tecnológico (CNPq), Financiadora de Estudos e Projeto (FINEP), Fundação de Amparo à Pesquisa do Estado de São Paulo (FAPESP);
- National Natural Science Foundation of China (NSFC), the Chinese Ministry of Education (CMOE) and the Ministry of Science and Technology of China (MSTC);
- Ministry of Education and Youth of the Czech Republic;
- Danish National Science Research Council and the Carlsberg Foundation;
- The European Research Council under the European Community’s Seventh Framework Programme;
- Helsinki Institute of Physics and the Academy of Finland;
- French CNRS-IN2P3, the ‘Region Pays de Loire’, ‘Region Alsace’, ‘Region Auvergne’ and CEA, France;
- German BMBF and the Helmholtz Association;
- Hungarian OTKA and National Office for Research and Technology (NKTH);
- Department of Atomic Energy and Department of Science and Technology of the Government of India;
- Istituto Nazionale di Fisica Nucleare (INFN) of Italy;
- MEXT Grant-in-Aid for Specially Promoted Research, Japan;
- Joint Institute for Nuclear Research, Dubna;
- Korea Foundation for International Cooperation of Science and Technology (KICOS);
- CONACYT, DGAPA, México, ALFA-EC and the HELEN Program (High-Energy physics Latin-American–European Network);
- Stichting voor Fundamenteel Onderzoek der Materie (FOM) and the Nederlandse Organisatie voor Wetenschappelijk Onderzoek (NWO), Netherlands;
- Research Council of Norway (NFR);
- Polish Ministry of Science and Higher Education;
- National Authority for Scientific Research - NASR (Autontatea Nationala pentru Cercetare Stiintifica - ANCS);
- Federal Agency of Science of the Ministry of Education and Science of Russian Federation, International Science and Technology Center, Russian Federal Agency of Atomic Energy, Russian Federal Agency for Science and Innovations and CERN-INTAS;
- Ministry of Education of Slovakia;
- CIEMAT, EELA, Ministerio de Educación y Ciencia of Spain, Xunta de Galicia (Consellería de Educación), CEADEN, Cubaenergía, Cuba, and IAEA (International Atomic Energy Agency);
- Swedish Research Council (VR) and Knut & Alice Wallenberg Foundation (KAW);
- Ukraine Ministry of Education and Science;
- United Kingdom Science and Technology Facilities Council (STFC);
- The United States Department of Energy, the United States National Science Foundation, the State of Texas, and the State of Ohio.

References

1. L. Evans and P. Bryant (editors), JINST **3** (2008) S08001
2. ALICE Collaboration, K. Aamodt et al., JINST **3** (2008) S08002
3. UA5 Collaboration, G.J. Alner et al., Z. Phys. C **33** (1986) 1
4. A.B. Kaidalov, Phys. Lett. B **116** (1982) 459; A.B. Kaidalov and K.A. Ter-Martirosyan, Phys. Lett. B **117** (1982) 247; A.B. Kaidalov and K.A. Ter-Martirosyan, Yad. Fiz. **39** (1984) 1545 and Sov. J. Nucl. Phys. **39** (1984) 979; A.B. Kaidalov and K.A. Ter-Martirosyan, Yad. Fiz. **40** (1984) 211 and Sov. J. Nucl. Phys. **40** (1984) 135
5. A. Capella et al., Z. Phys. C **3** (1980) 329; A. Capella and J. Tran Thanh Van, Z. Phys. C **10** (1981) 249; A. Capella and J. Tran Thanh Van, Phys. Lett. B **114** (1982) 450; A. Capella, U. Sukhatme, C.-I. Tan and J. Tran Thanh Van, Phys. Rep. **236** (1994) 225
6. N.S. Amelin and L.V. Bravina, Yad. Fiz. **51** (1990) 211 and Sov. J. Nucl. Phys. **51** (1990) 133; N.S. Amelin et al., Yad. Fiz. **51** (1990) 512 and Sov. J. Nucl. Phys. **51** (1990) 327; N.S. Amelin et al., Yad. Fiz. **52** (1990) 272 and Sov. J. Nucl. Phys. **51** (1990) 172
7. P. Aurenche et al., Phys. Rev. D **45** (1992) 92
8. R. Engel, J. Ranft and S. Roesler, Phys. Rev. D **52** (1995) 1459
9. J.G. Rushbrooke and B.R. Webber, Phys. Rep. C **44** (1978) 1
10. UA5 Collaboration, K. Alpgård et al., Phys. Lett. B **112** (1982) 183; M. Ambrosio et al., AIP Conference Proceedings **85** (1982) 602
11. T. Antičić et al., ALICE Internal Note ALICE-INT-2005-015 (2005); T. Antičić et al. (ALICE Collaboration), J. Phys. Conf. Series **119** (2008) 022006
12. ALICE Collaboration, AliRoot, ALICE Offline simulation, reconstruction and analysis framework, <http://aliceinfo.cern.ch/Offline/>
13. T.M. Steinbeck (ALICE Collaboration), Proceedings of CHEP 2009, March 2009, Prague, to be published in J. Phys. Conf. Series
14. ALICE Collaboration, J. Phys. G **30** (2004) 1517 and J. Phys. G **32** (2006) 1295
15. P.G. Kuijer (ALICE Collaboration), Nucl. Phys. A **830** (2009) 81C; F. Prino (ALICE Collaboration), Nucl. Phys. A **830** (2009) 527C; R. Santoro et al. (ALICE Collaboration), JINST **4** (2009) P03023; G. Aglieri Rinella et

- al, CERN preprint CERN-2008-008 (2008); P. Giubellino (ALICE Collaboration), Proceedings of EPS HEP 2009, July 2009 Krakow, to be published in Proc. of Science
16. C. Bombonati et al., ALICE Internal Note ALICE-INT-2009-035 (2009)
 17. T. Sjöstrand, *Comput. Phys. Commun.* **82** (1994) 74; T. Sjöstrand, S. Mrenna and P. Skands, *JHEP* **2006** 05 (2006) 026
 18. M.G. Albrow et al. (Tev4LHC QCD Working Group), arXiv:hep-ph/0610012 (2006), D6T (109) tune
 19. UA5 Collaboration, R.E. Ansorge et al., *Z. Phys. C* **33** (1986) 175
 20. E. Bruna et al., ALICE Internal Note ALICE-INT-2009-018 (2009)
 21. D. Elia, et al., ALICE Internal Note ALICE-INT-2009-021 (2009)
 22. J.F. Grosse-Oetringhaus et al., ALICE Internal Note ALICE-INT-2009-022 (2009)
 23. R. Brun et al., 1985 GEANT3 User Guide, CERN Data Handling Division DD/EE/841; R. Brun et al., 1994 CERN Program Library Long Write-up, W5013, GEANT Detector Description and Simulation Tool
 24. J.F. Grosse-Oetringhaus, PhD thesis, University of Münster, Germany (2009), CERN-THESIS-2009-033
 25. A.B. Kaidalov and M.G. Poghosyan, submitted to *Eur. Phys. J. C*, arXiv:0910.2050 [hep-ph] (2009)
 26. A. Moraes (ATLAS Collaboration), ATLAS Note ATL-COM-PHYS-2009-119 (2009), ATLAS CSC (306) tune
 27. P.Z. Skands, Multi-Parton Interaction Workshop, Perugia, Italy, 28-31 Oct 2008, arXiv:0905.3418 [hep-ph] (2009), Perugia-0 (320) tune
 28. W. Thome et al., *Nucl. Phys. B* **129** (1977) 365
 29. UA1 Collaboration, C. Albajar et al., *Nucl. Phys. B* **335** (1990) 261
 30. UA5 Collaboration, G.J. Alner et al., *Phys. Rep.* **154** (1987) 247
 31. CDF Collaboration, F. Abe et al., *Phys. Rev. D* **41** (1990) 2330